

Electronic Supporting Information

A small-molecule probe to decipher stress-induced ER microenvironments and ER-Golgi communication†

Tanoy Dutta,^{*a,b} Barsha Chakraborty,^a Aditya Nigam,^c Shilpi Minocha,^c and Apurba Lal Koner^{*a}

^a Bionanotechnology Lab, Department of Chemistry, Indian Institute of Science Education and Research Bhopal, Bhopal Bypass Road, Bhauri, Bhopal, Madhya Pradesh - 462066, INDIA. E-mail: akoner@iiserb.ac.in

^b Division of Cardiovascular Medicine, Brigham and Women's Hospital, Harvard Medical School, Boston, MA 02115, USA. E-mail: tdutta2@bwh.harvard.edu

^c Kusuma School of Biological Sciences, Indian Institute of Technology Delhi, Hauz Khas, New Delhi - 110016, India

Experimental Section/Methods

Materials and Methods:

All the solvents and reagents were procured from commercial sources and used without any further purification. The spectroscopic grade solvents were purchased from Sisco Research Laboratories Pvt. Ltd. (SRL), India. 4-Chloro-7-nitrobenzofurazan (ER-Cl) and CDCl_3 were purchased from Sigma Aldrich (USA). Butylamine, hexylamine, and octylamine were purchased from Alfa Aesar (USA). Dulbecco's Modified Eagle Medium (DMEM), L-Glutamine-Penicillin-Streptomycin solution (antibiotic cocktail), and Fetal Bovine Serum (FBS) were purchased from HiMedia (USA). Lyso-Tracker Red, MitoTracker Red, and ER Tracker Red were purchased from Thermo Fisher Scientific (USA). LipidSpot 610 was purchased from Biotium (USA). Brefeldin A was purchased from Sigma Aldrich (USA). 5-fluorouracil was purchased from Avra Synthesis Pvt. Ltd. (India). The spectroscopic experiments in water were carried out using Milli-Q grade water using Milli-Q water purification set up from Merck (USA) with resistivity $18.2 \text{ M}\Omega \cdot \text{cm}$ at 298 K. Thin layer chromatography (TLC) was performed using Merck Silica gel 60 F-254 pre-coated plates and visualized using UV-irradiation ($\lambda = 254/365 \text{ nm}$).

Silica gel from Merck (particle size 100-200 mesh) was used for column chromatography. ^1H and ^{13}C -NMR spectra were recorded on a Bruker 500 MHz spectrometer with operating frequencies of 126 MHz for ^{13}C . Chemical shifts (δ) are reported in ppm relative to the residual solvent signal ($\delta = 7.26$ for ^1H NMR and $\delta = 77.0$ for ^{13}C NMR). High-resolution mass spectrometry (HRMS) data were recorded on Bruker MicrOTOF-Q-II mass spectrometer using chloroform as the solvent. All absorption spectra and fluorescence measurements were carried out using SHIMADZU 1800 UV-Vis. spectrophotometer and HORIBA Jobin Yvon Fluorolog 3 equipped with a 450 W Xe arc lamp using 1 cm path length quartz cuvettes. Both excitation and emission slit widths were kept at 1 nm while recording the emission spectra. The absolute quantum yields in solution were measured using QuantaPhi integrating sphere luminescence yield system (HORIBA).

Cell Culture and Microscopy:

BHK-21, A549, MDA-MB-231, HeLa, and HepG2 cells were obtained from the National Center for Cell Science (NCCS), India and were grown in a 25 cm² cell culture flask in DMEM (phenol red free) containing 10% (v/v) FBS and 1% (v/v) antibiotic cocktail in 5% CO₂ at 37 °C in the incubator. For imaging purposes, cells were grown to 80% confluency in the 35 mm glass-bottom imaging dishes ($170 \pm 5 \mu\text{m}$). The cells were co-incubated with 2 μM of the probe of interest and 0.3 μM of Lyso-Tracker Red / ER-Tracker Red / MitoTracker Red (whichever is applicable) for 10 minutes and washed with PBS (pH 7.4) twice before imaging. No washing step was performed in cases of incubation with alkylated ER dyes only.

Tissue Sample Preparation:

Wild-type liver tissues were collected from 10-to-14-week-old male mice. After collection, the tissues were paraffin-embedded and, subsequently, sectioned into 4 μm thick sections using a rotary microtome. Before staining, the paraffin-embedded sections were first (i) deparaffinized in xylene, (ii) rehydrated through graded ethanol washes, and (iii) rinsed twice with 1X PBS (pH 7.4).

ER Isolation:

The ER isolation method is described stepwise. i) Cells were grown in a complete monolayer at high density. ii) The cells were scraped and taken in 1X PBS 7.4 (137 mM NaCl, 2.7 mM KCl, 10 mM Na₂HPO₄, 1.8 mM KH₂PO₄) on ice. iii) Sedimentation of cells @ 3000 rpm in swinging bucket rotor. iv) PBS was aspirated and 5 mM Hepes 7.4 was added. Any visible clumps were removed carefully. v) Cell lysis was performed by swelling the cells on ice. After 90% lysis, 5 mM MgCl₂, 100 mM KAc, and 1X complete protease inhibitor were added. vi) The solution was fixed thoroughly and swung @ 3000 rpm to remove nuclei and non-lysed cells. vii) Further centrifugation of the supernatant was performed @ 12,000 rpm to pellet down mitochondria, lysosomes, and endosomes. viii) The pellets were removed and the supernatant was ultracentrifuged using MLA-80 tubes @ 70,000 for 1 h to obtain the ER pellet. ix) Finally, the pellet was put in membrane buffer (100 mM KAc, 50 mM HEPES, 5 mM MgCl₂, 250 mM sucrose), stained with the dye of interest, and imaged using a confocal microscope.

Confocal Microscopy:

All the confocal microscopy imaging was performed with an Olympus FV3000 Confocal Laser Scanning Microscope (LSM). The image processing was done with the help of cellSens software (Olympus). For imaging, 488 nm (for the developed ER-staining probes), 561 nm (ER/Lyso/Mito Tracker Red), and 594 nm (LipidSpot 610) excitation lasers were used. The confocal aperture was kept at 1.0 Airy Disk (AU) while the dwell time was maintained at 8 μs/pixel for all the imaging experiments. The laser power, gain, and offset were kept the same in all cases. The emission window was kept as 500 – 540 nm, 570 – 620 nm, and 600 – 640 nm for the excitation of 488 nm (0.5% of laser power), 561 nm (0.5% of laser power), and 594 nm respectively (1% of laser power). The images were acquired in sequential scan mode ensuring zero cross-talk between the imaging channels.

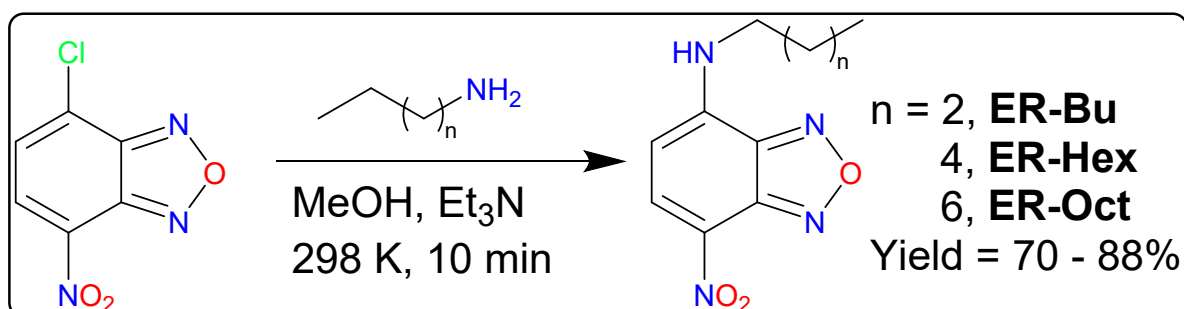
Fluorescence Lifetime Imaging Microscopy (FLIM):

For the FLIM experiment, live BHK-21 cells were grown in 35 mm glass bottom imaging dishes for 24 h at a density of $2 \times 10^5 \cdot \text{mL}^{-1}$. The experiment was performed in a PicoQuant MicroTime 200 Time-resolved Fluorescent Microscope with a UPLSAPO 60X PlanApochromat, NA 1.42,

water immersion objective. A single-mode pulsed diode laser (530 nm with a pulse width of ~ 240 ps in full width at half maximum and average power of ~ 10 μ W) was used as an excitation source. A dichroic mirror (Z532 RDC, AHF), a long pass filter (HQ530lp, AHF), a 50 μ m pinhole, and an avalanche photodiode detector were used to collect emissions from cells. The measurement was performed multiple times for both samples. Time-resolved fluorescence decay curves were obtained from FLIM images and fluorescence lifetimes were evaluated according to non-linear least-squares iterative curve fitting using the DecayFit Emission Decay Analysis Software (FluorTools) v1.4.

Synthesis of ER-staining Dyes:

A solution of 4-Chloro-7-nitrobenzofurazan (100 mg, 0.501 mmol) was prepared in 10 mL methanol. To that solution, 1.002 mmol of butylamine/ hexylamine/ octylamine was added dropwise followed by the addition of 20 μ L triethylamine. Upon stirring at 298 K for 10 minutes, the color of the solution changed from pale yellow to dark brown and the progress of the reaction was checked by thin-layer chromatography. Then the solvent was removed under reduced pressure and the residue was purified by silica gel column chromatography using a 30 – 40% mixture of ethyl acetate and hexane as eluent and the yield was calculated ranging from 70% to 88% for different alkylated-ER derivatives.



Scheme S1: Synthetic route to develop ER-staining probes.

^1H NMR, ^{13}C NMR, and HRMS data:

N-butyl-7-nitrobenzo[c][1,2,5]oxadiazol-4-amine (ER-Bu): ^1H NMR (Chloroform-*d*, 500 MHz) δ (ppm) 8.50 (d, $J = 8.6$ Hz, 1H), 6.21 (br. s, 1H), 6.18 (d, $J = 8.6$ Hz, 1H), 3.50 (q, $J = 6.7$ Hz, 2H), 1.86 – 1.75 (m, 3H), 1.56 – 1.46 (m, 2H), 1.02 (t, $J = 7.3$ Hz, 3H). ^{13}C NMR (Chloroform-*d*, 125

MHz) δ (ppm) 144.26, 143.88, 143.78, 136.50, 123.98, 98.49, 43.71, 30.54, 20.14, 13.67. HRMS (ESI) m/z : $[M + H]^+$ calcd. for $C_{10}H_{13}N_4O_3$ 237.0988; found, 237.0982.

N-hexyl-7-nitrobenzo[*c*][1,2,5]oxadiazol-4-amine (**ER-Hex**): Yield = 79%. 1H NMR (Chloroform-*d*, 500 MHz) δ (ppm) 8.50 (d, $J = 8.6$ Hz, 1H), 6.21 (br. s, 1H), 6.17 (d, $J = 8.6$ Hz, 1H), 3.49 (q, $J = 6.8$ Hz, 2H), 1.85 – 1.78 (m, 2H), 1.52 – 1.44 (m, 2H), 1.40 – 1.33 (m, 4H), 0.92 (t, $J = 7.0$ Hz, 3H). ^{13}C NMR (Chloroform-*d*, 125 MHz) δ (ppm) 144.27, 143.89, 143.82, 136.47, 124.05, 98.48, 44.00, 31.36, 28.53, 26.62, 22.51, 13.97. HRMS (ESI) m/z : $[M + Na]^+$ calcd. for $C_{12}H_{16}N_4O_3Na$ 287.1120; found, 287.1115.

N-octyl-7-nitrobenzo[*c*][1,2,5]oxadiazol-4-amine (**ER-Oct**): Yield = 88%. 1H NMR (Chloroform-*d*, 500 MHz) δ (ppm) 8.50 (d, $J = 8.6$ Hz, 1H), 6.20 (br. s, 1H), 6.17 (d, $J = 8.6$ Hz, 1H), 3.52 – 3.45 (q, 2H), 1.86 – 1.77 (m, 2H), 1.51 – 1.44 (m, 2H), 1.40 – 1.27 (m, 8H), 0.88 (t, $J = 7.0$ Hz, 2H). ^{13}C NMR (Chloroform-*d*, 125 MHz) δ (ppm) 144.41, 144.04, 143.99, 136.63, 124.14, 98.63, 44.15, 31.87, 29.31, 29.26, 28.69, 27.09, 22.75, 14.21. HRMS (ESI) m/z : $[M + Na]^+$ calcd. for $C_{14}H_{20}N_4O_3Na$ 315.1535; found, 315.1428.

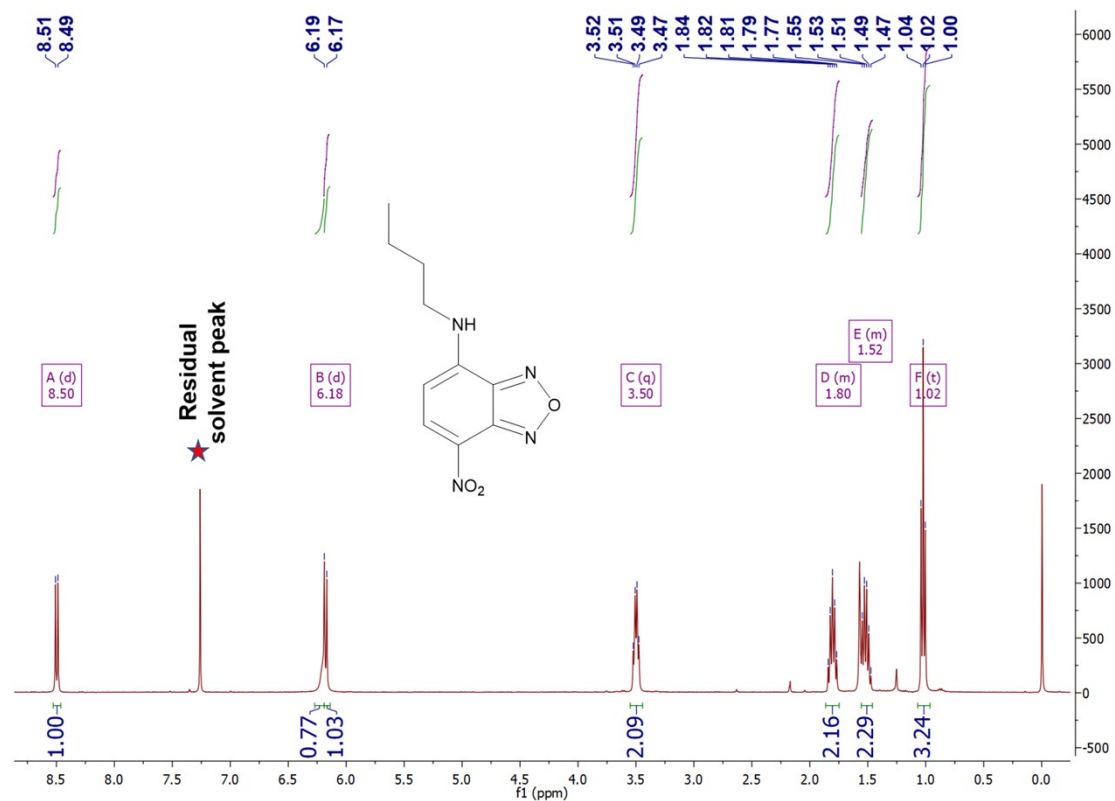


Fig. S1. 1H NMR spectra (500 MHz) of **ER-Bu** in $CDCl_3$.

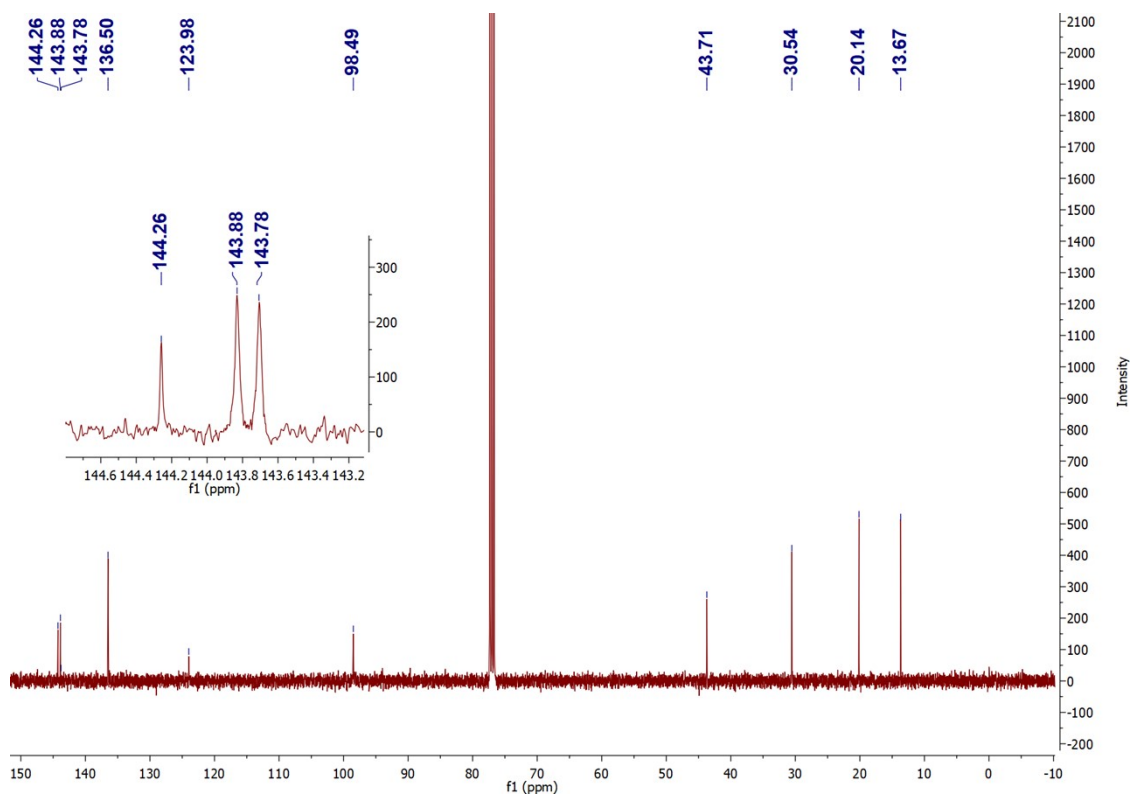


Fig. S2. ¹³C NMR spectra (125 MHz) of ER-Bu in CDCl₃.

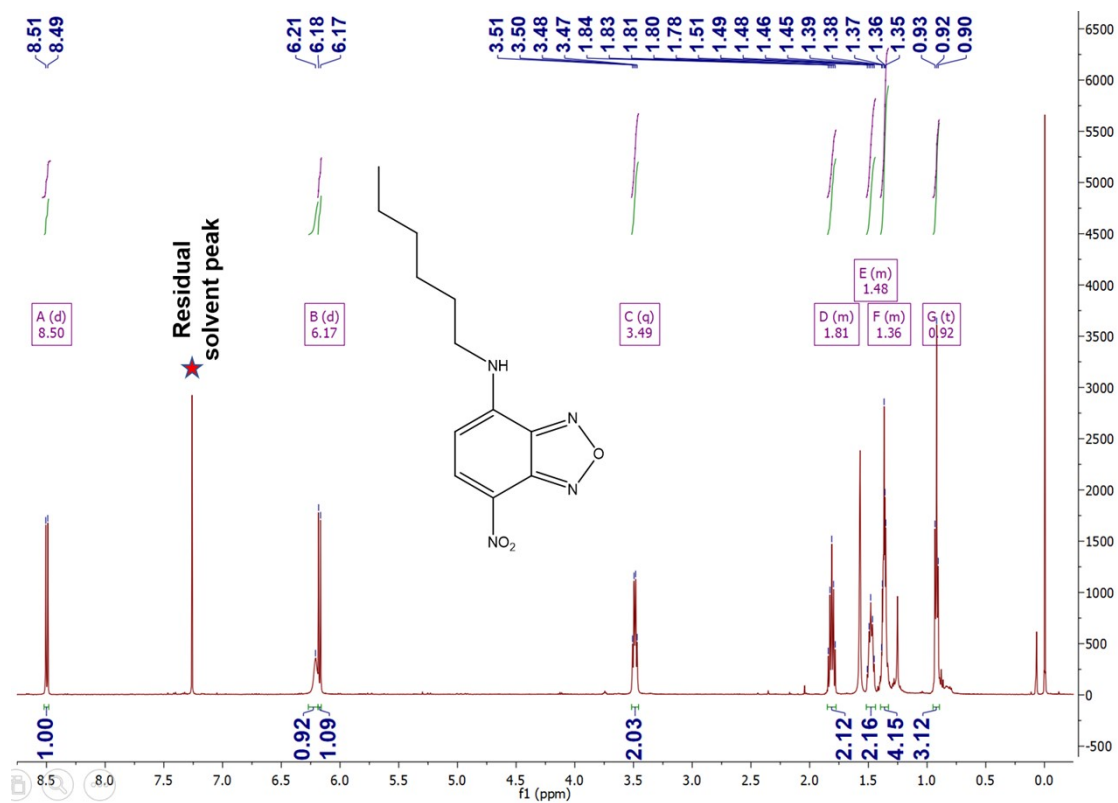


Fig. S3. ¹H NMR spectra (500 MHz) of ER-Hex in CDCl₃.

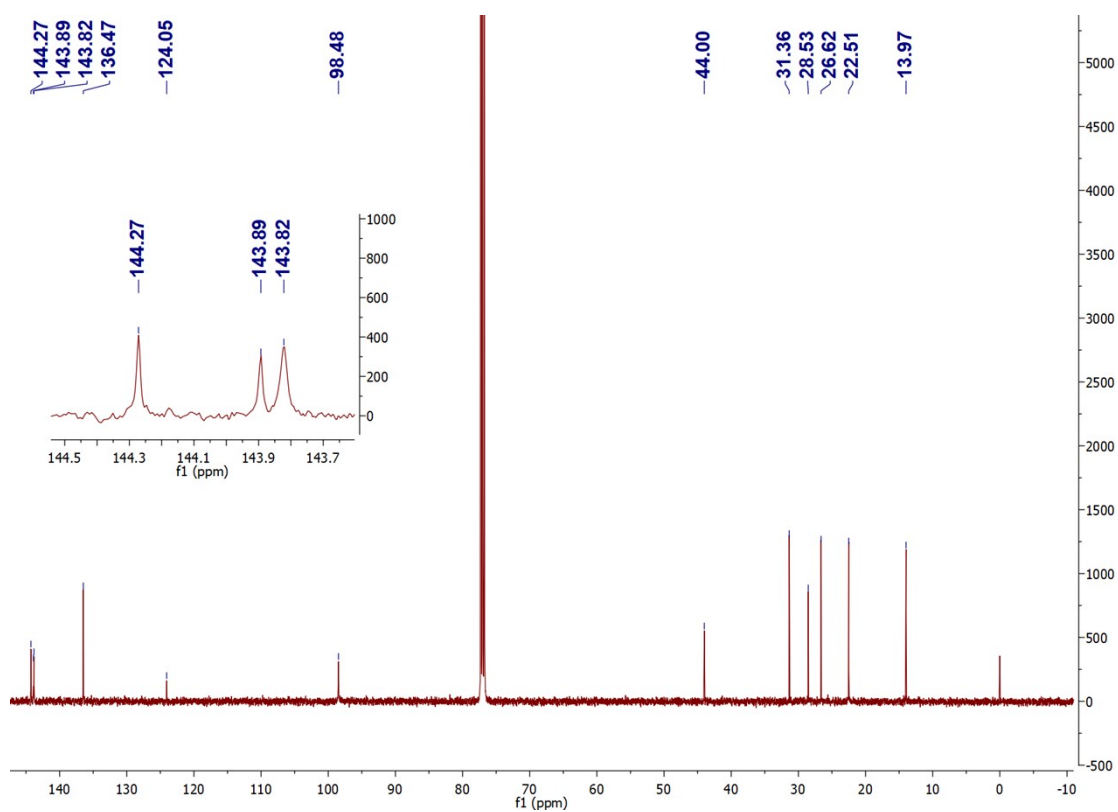


Fig. S4. ¹³C NMR spectra (125 MHz) of ER-Hex in CDCl₃.

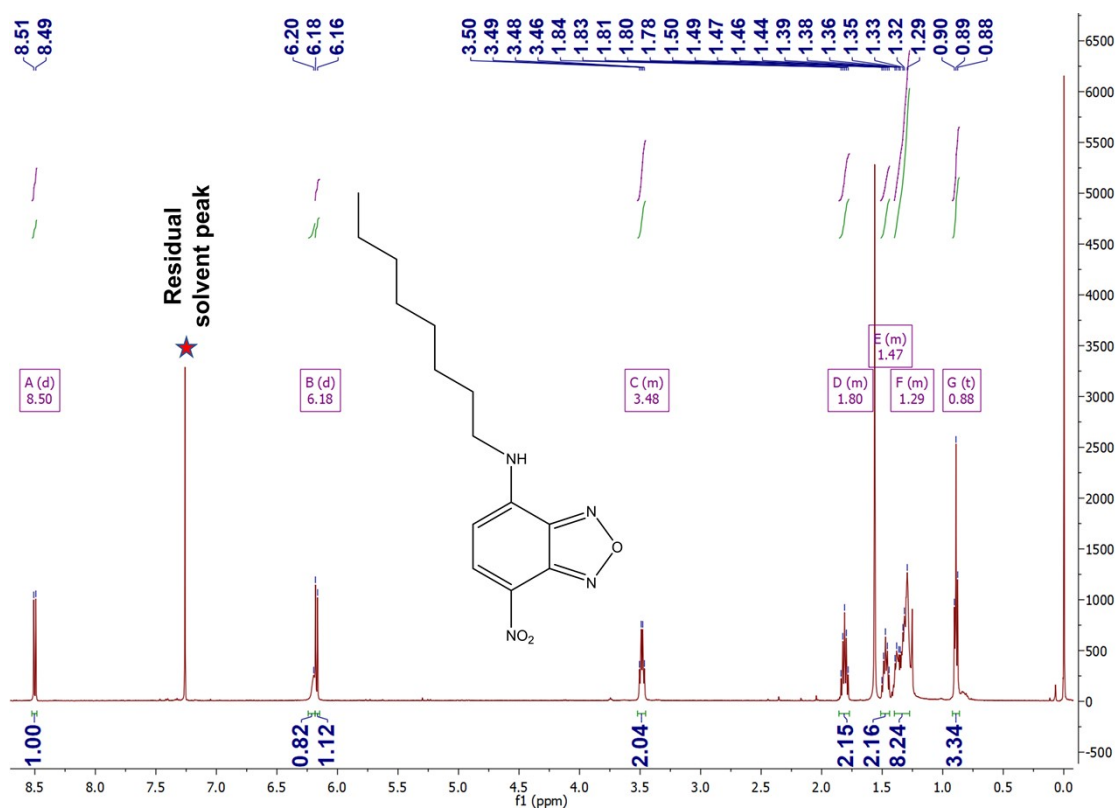


Fig. S5. ¹H NMR spectra (500 MHz) of ER-Oct in CDCl₃.

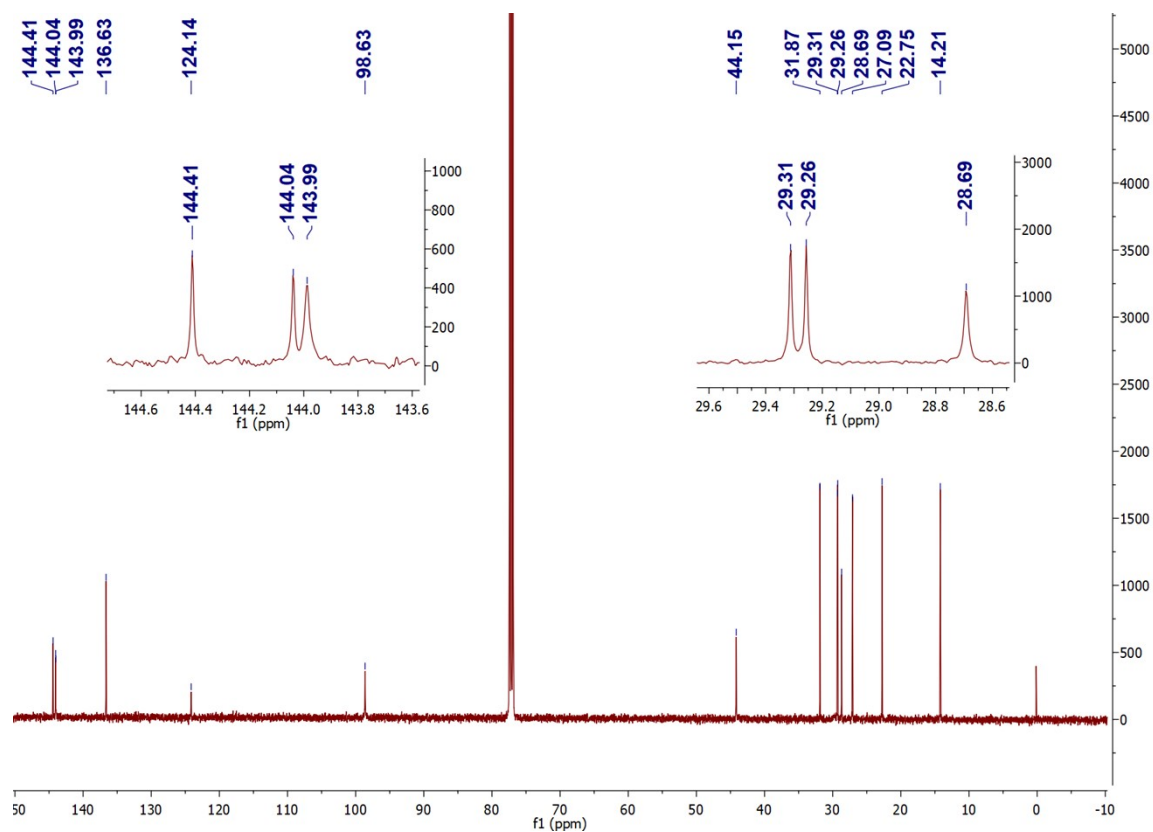


Fig. S6. ^{13}C NMR spectra (125 MHz) of ER-Oct in CDCl_3 .

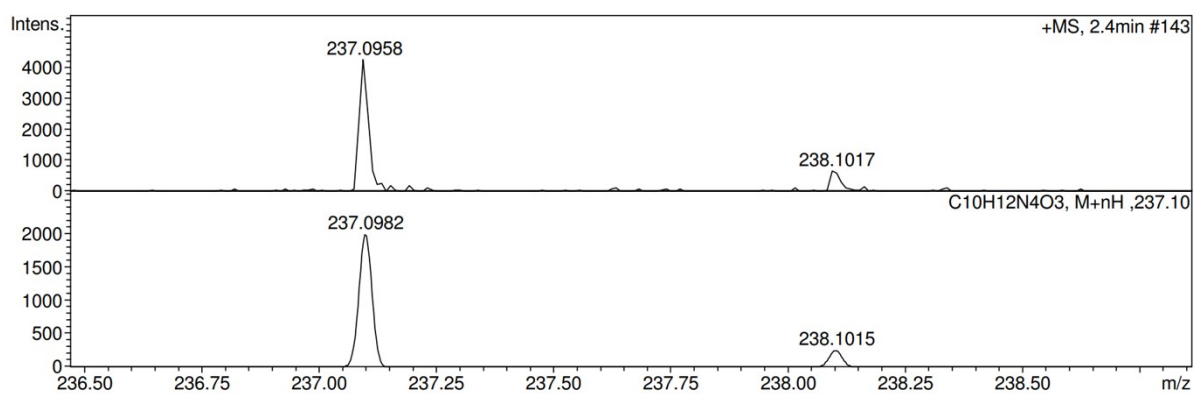


Fig. S7. High-resolution mass spectrum (HRMS) of ER-Bu. Expected mass $[M/Z]$: 237.0988 Da and obtained mass is 237.0982 Da $[(M+H)/Z]$.

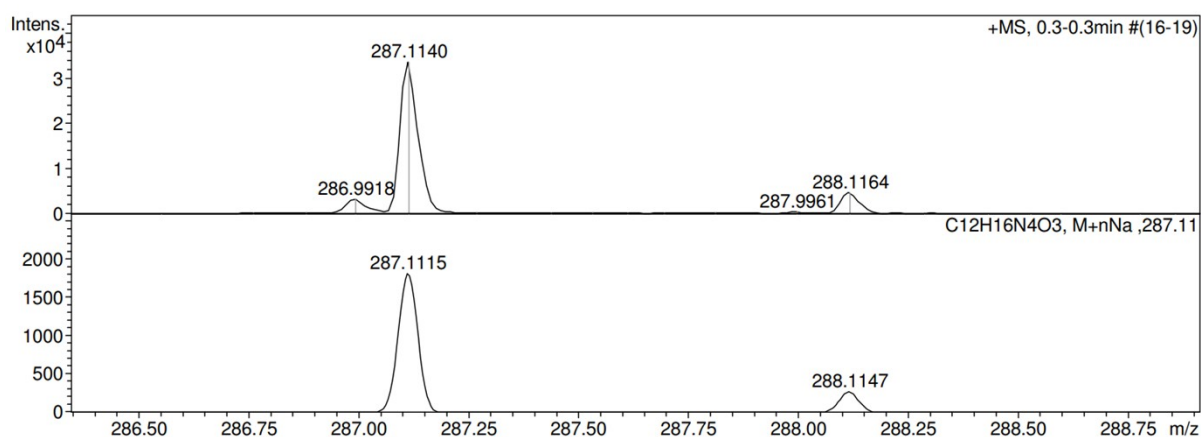


Fig. S8. High-resolution mass spectrum (HRMS) of ER-Hex. Expected mass $[M/Z]$: 287.1120 Da and obtained mass is 287.1115 Da $[(M+Na)/Z]$.

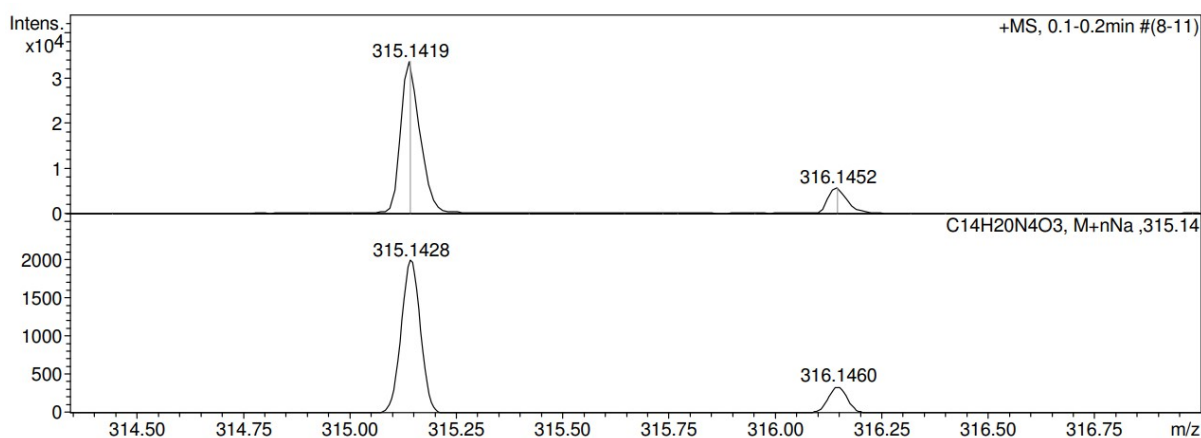


Fig. S9. High-resolution mass spectrum (HRMS) of ER-Oct. Expected mass $[M+Na/Z]$ = 315.1535 Da and obtained mass is 315.1428 Da $[(M+Na)/Z]$.

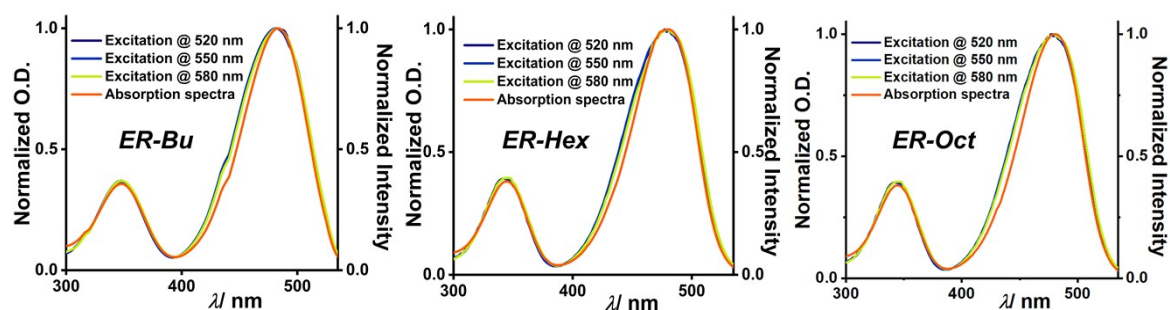


Fig. S10. Overlapping absorption and excitation spectra (monitored at different wavelengths) of the probes (5 μ M) in water confirm their spectroscopic purity.

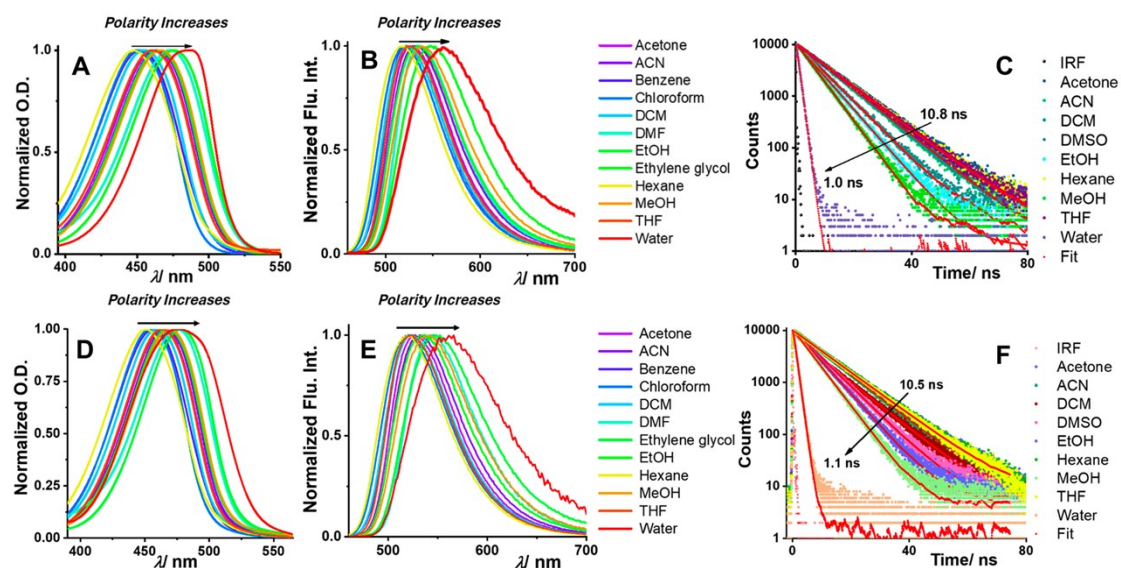


Fig. S11. (A) UV-Visible, (B) emission spectra, and (C) fluorescence lifetime decays of **ER-Bu** (5 μM); (D) UV-Visible, (E) emission spectra, and (F) fluorescence lifetime decays of **ER-Hex** (5 μM) in different polar solvents.

Table S1. Spectroscopic properties of **ER-Bu** in solvents of various polarity (ascending order, from low to high polarity)

Solvents	λ_{abs}^{max} /nm	λ_{em}^{max} /nm	Stokes shift /nm	$\langle \tau \rangle$ / ns	Abs. QY (%)	$E_T(30)^{[1]}$
Hexane	448	520	72	10.8	46.23	31.0
Benzene	452	522	70	9.6	43.14	34.3
THF	461	524	63	9.8	32.43	37.4
Chloroform	452	527	67	8.8	61.22	39.1
DCM	456	523	67	9.2	37.89	40.7
Acetone	462	528	66	10.5	32.95	42.2
DMF	473	538	65	8.2	21.96	43.2

ACN	463	533	70	8.2	38.13	45.6
Ethanol	465	532	67	6.3	19.34	51.9
Methanol	467	539	72	5.0	10.72	55.5
Ethylene glycol	476	552	76	4.5	6.24	56.3
Water	484	565	81	1.0	0.29	63.0

Table S2. Spectroscopic properties of **ER-Hex** in solvents of various polarity (ascending order, from low to high polarity)

Solvents	λ_{abs}^{max} /nm	λ_{em}^{max} /nm	Stokes shift /nm	$\langle\tau\rangle$ / ns	Abs. QY (%)	$E_T(30)^{[1]}$
Hexane	448	520	72	10.5	47.79	31.0
Benzene	452	522	70	9.7	44.31	34.3
THF	461	524	63	9.7	34.12	37.4
Chloroform	452	527	67	8.8	63.38	39.1
DCM	456	523	67	9.1	39.45	40.7
Acetone	462	528	66	10.4	34.16	42.2
DMF	473	538	65	8.1	22.43	43.2
ACN	463	533	70	8.3	39.54	45.6
Ethanol	465	532	67	6.2	21.19	51.9
Methanol	467	539	72	5.2	12.87	55.5
Ethylene glycol	476	552	76	4.5	6.98	56.3
Water	484	565	81	1.1	0.32	63.0

Table S3. Spectroscopic properties of **ER-Oct** in solvents of various polarity (ascending order, from low to high polarity)

Solvents	λ_{abs}^{max} /nm	λ_{em}^{max} /nm	Stokes shift /nm	$\langle\tau\rangle$ / ns	Abs. QY (%)	$E_T(30)^{[1]}$
Hexane	448	520	72	10.6	52.87	31.0
Benzene	452	522	70	9.7	45.56	34.3
THF	461	524	63	9.8	34.67	37.4
Chloroform	452	527	67	8.7	65.24	39.1
DCM	456	523	67	9.2	43.36	40.7
Acetone	462	528	66	10.4	35.67	42.2
DMF	473	538	65	8.1	24.13	43.2
ACN	463	533	70	8.2	40.72	45.6
Ethanol	465	532	67	6.1	22.51	51.9
Methanol	467	539	72	5.2	13.5	55.5
Ethylene glycol	476	552	76	4.5	7.57	56.3
Water	484	565	81	0.9	0.34	63.0

pH stability of ER-Oct:

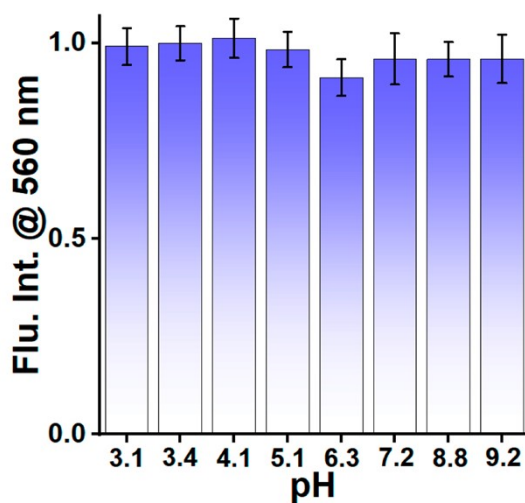


Fig. S12. Fluorescence intensity of **ER-Oct** at 560 nm ($\lambda_{ex} = 480$ nm) against pH (3-9).

Cytotoxicity assay of ER-Bu and ER-Hex in BHK-21 cell line:

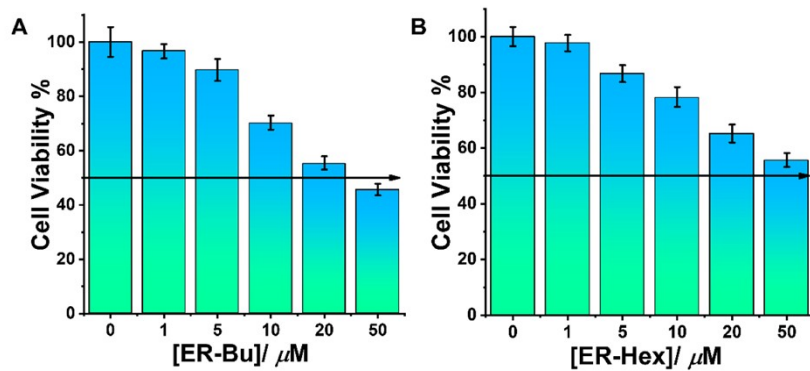


Fig. S13. Cytotoxicity assay of (A) ER-Bu and (B) ER-Hex performed BHK-21 cell line for 24 h.

Cytotoxicity assay of ER-Oct in different cell lines:

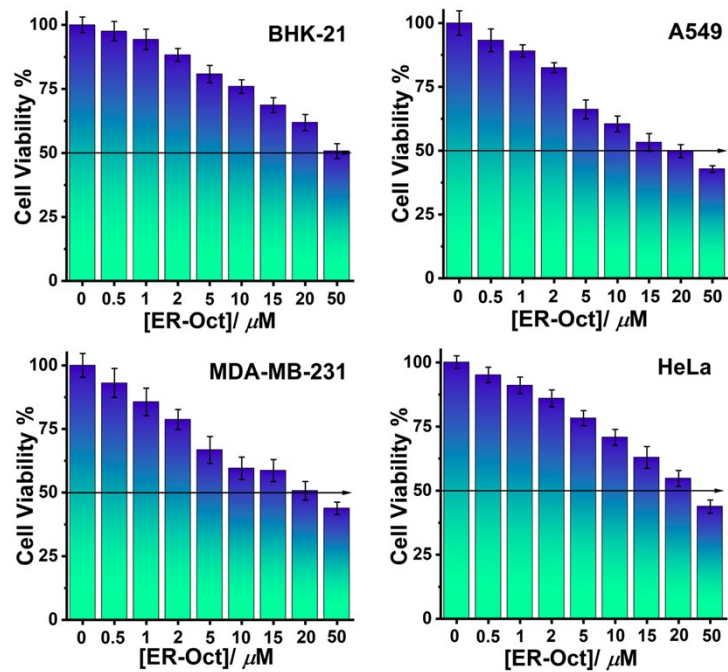


Fig. S14. Cytotoxicity assay of ER-Oct performed in (A) BHK-21, (B) A549, (C) MDA-MB-231, and (D) HeLa cell lines for 24 h.

Sub-cellular localization of the probes:

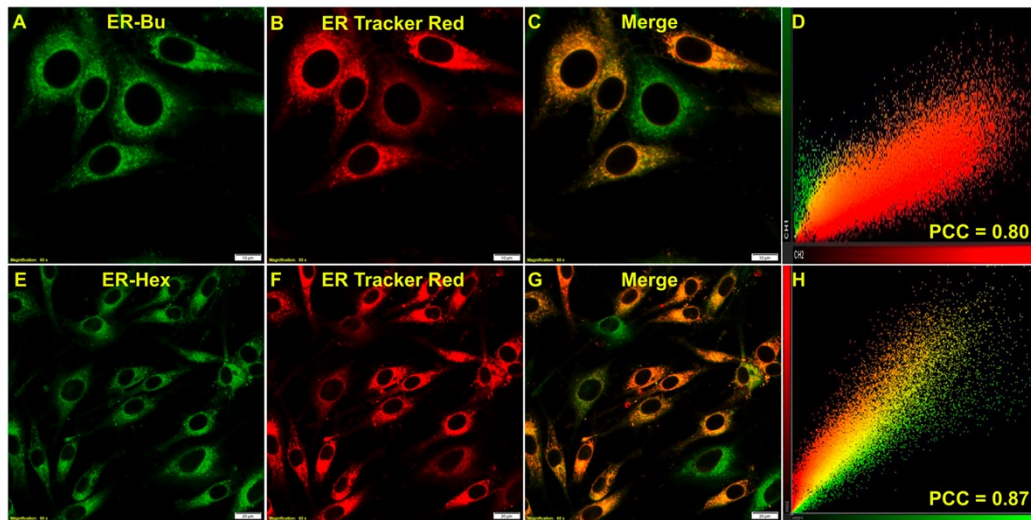


Fig. S15. CLSM images of BHK-21 cells show localization of **ER-Bu** and **ER-Hex**. The cells stained with (A) 2 μM **ER-Bu**, (B) 0.3 μM ER Tracker Red, (C) merge image, (D) corresponding scatter plot (scale bar: 10 μm); (E) 2 μM **ER-Hex**, (F) 0.3 μM ER Tracker Red, (G) merge image, (H) corresponding scatter plot (scale bar: 20 μm).

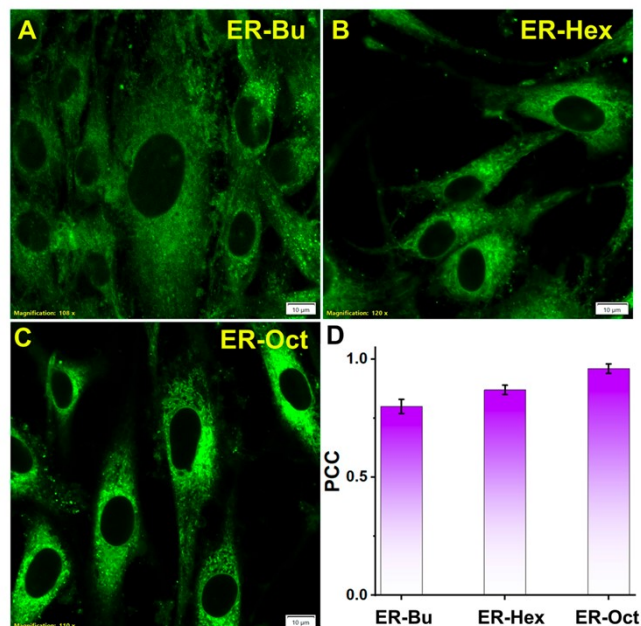


Fig. S16. CLSM images of live BHK-21 cells stained with 2 μM (A) **ER-Bu**, (B) **ER-Hex**, and (C) **ER-Oct** (scale bar: 10 μm). (D) shows the bar plot comparing the Pearson's correlation coefficient (PCC) values obtained for three different probes.

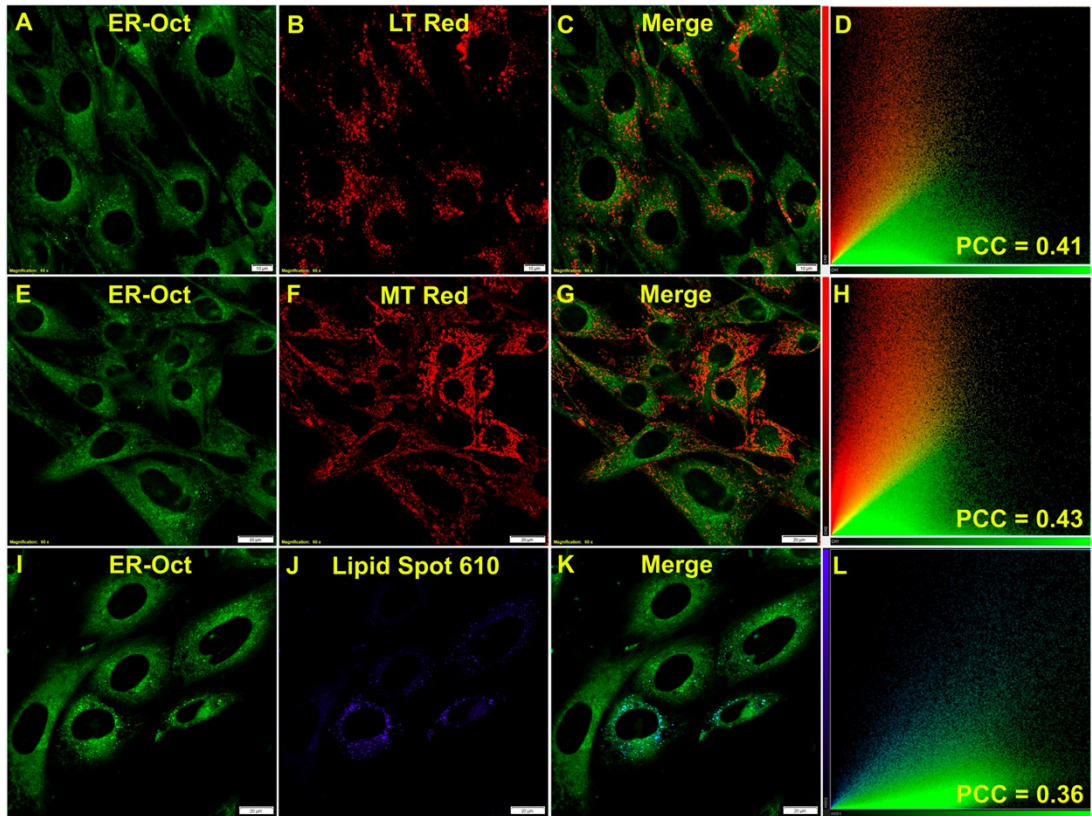


Fig. S17. CLSM images of live BHK-21 cells stained with (A) 2 μM ER-Oct, (B) 0.3 μM LysoTracker Red, (C) merge image of (A) and (B), (D) scatter plot showing Pearson's coefficient 0.41 ± 0.02 (scale bar: 10 μm); (E) 2 μM ER-Oct, (F) 0.3 μM MitoTracker Red, (G) merge image of (E) and (F), and (H) scatter plot showing Pearson's coefficient 0.43 ± 0.03 (scale bar: 20 μm); (I) 2 μM ER-Oct, (J) 0.3 μM LipidSpot 610, (K) merge image of (I) and (J), (L) scatter plot showing Pearson's coefficient 0.36 ± 0.02 (scale bar: 20 μm).

Rapid internalization of ER-Oct in live cells

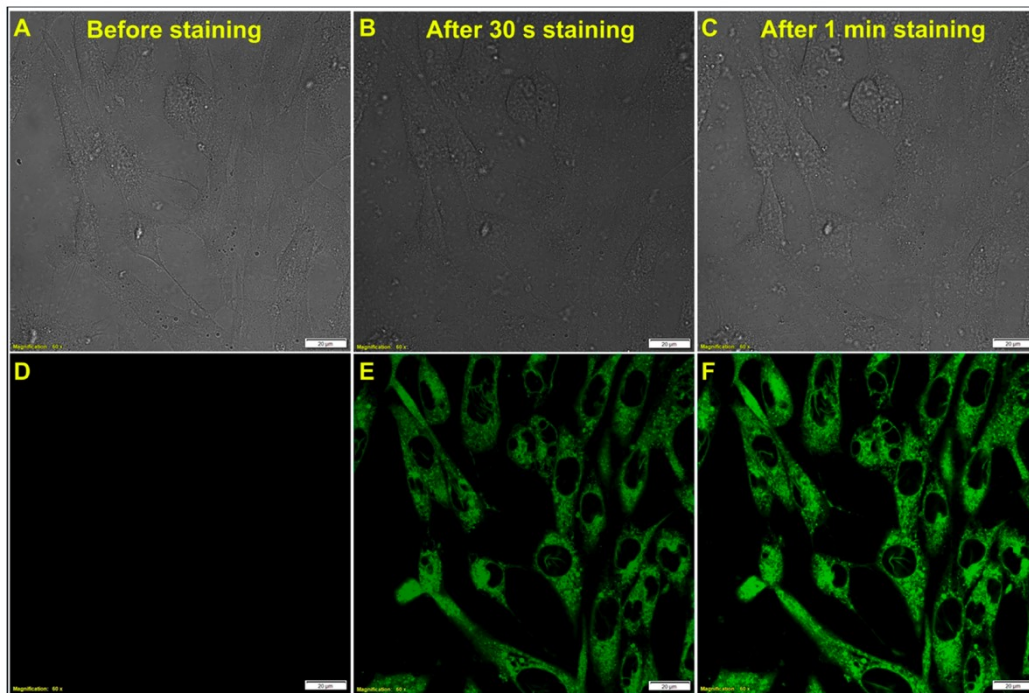


Fig. S18. CLSM images of BHK-21 cells stained with 2 μ M **ER-Oct** show the super-fast localization (wash-free) inside ER. (A-C) are the DIC images; (D-F) show images before staining, after 30 s staining, and after 1 min staining with **ER-Oct**, respectively.

Photostability in biological systems:

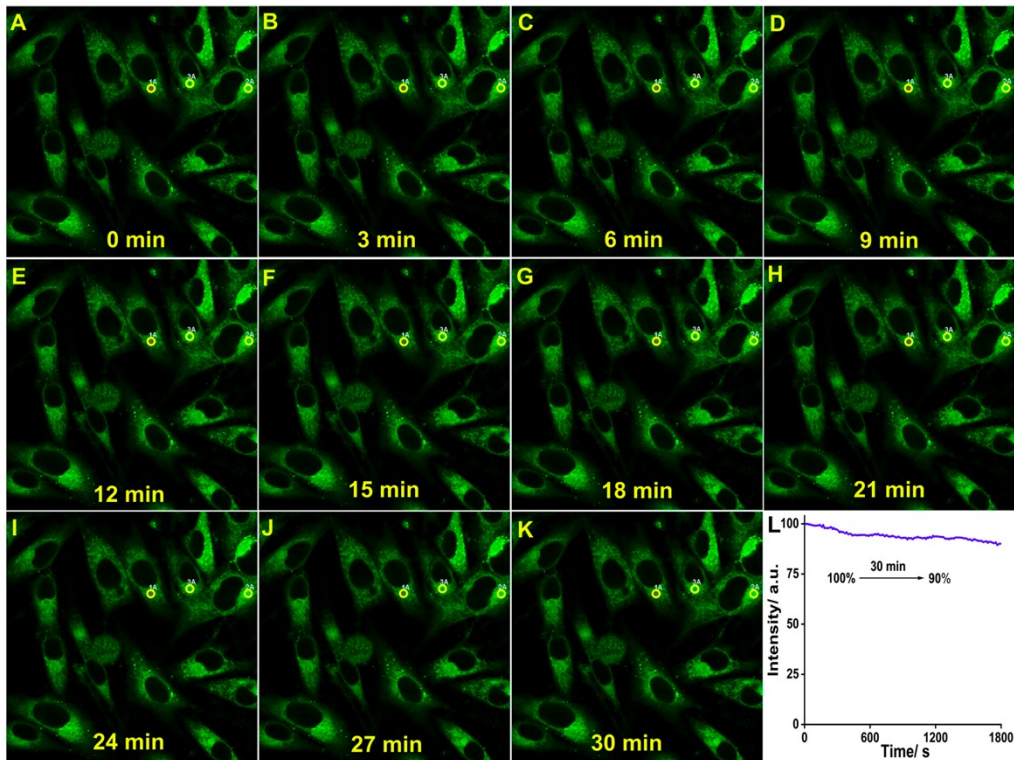


Fig. S19. Photostability of ER-Oct demonstrated by the time-lapse imaging of BHK-21 cells stained with 2 μ M ER-Oct. (A-K) show images at different time points and (L) corresponding plot of intensity vs. time (30 min).

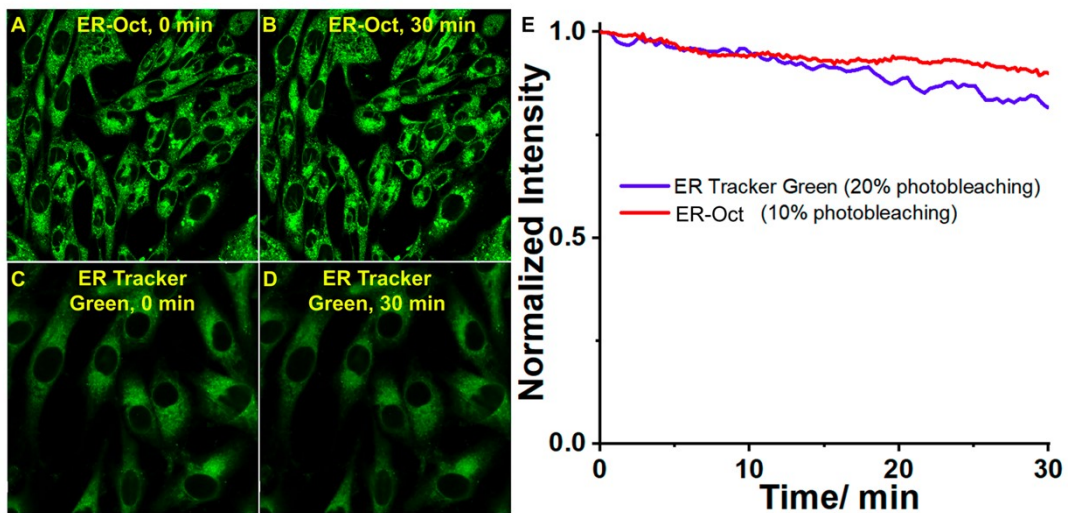


Fig. S20. CLSM images of BHK-21 cells stained with (A-B) ER-Oct and (C-D) ER Tracker Green (E) intensity vs. time plot demonstrating the photostability of ER-Tracker Green and ER-Oct obtained from the time-lapse imaging.

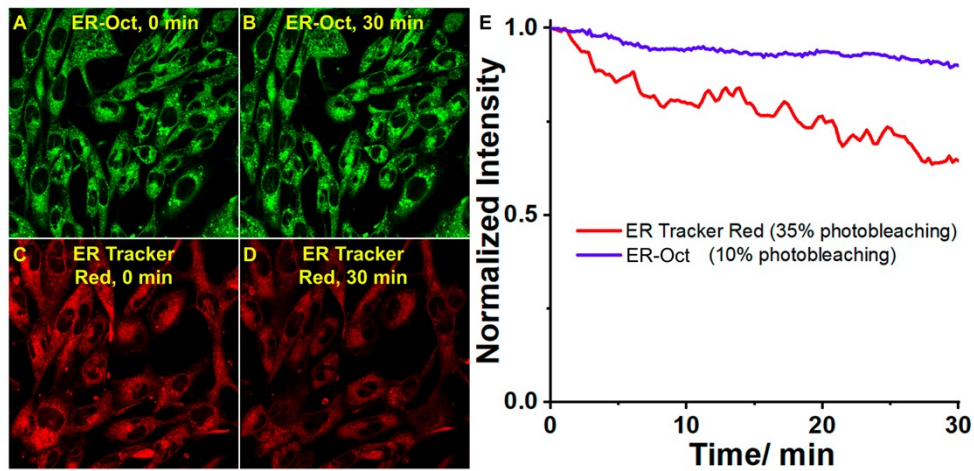
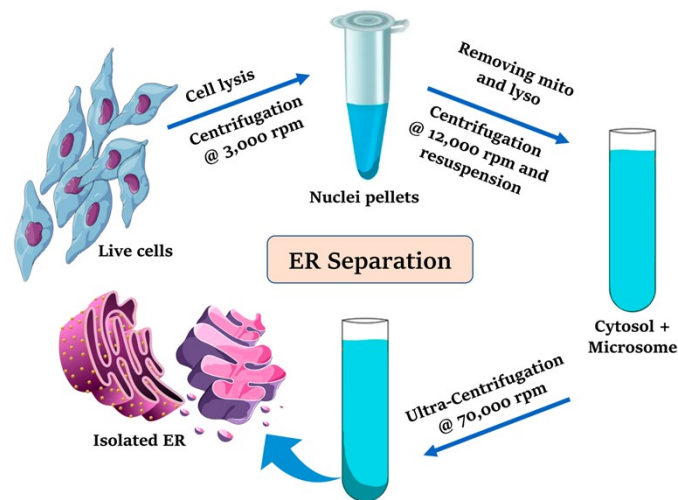


Fig. S21. CLSM images of BHK-21 cells stained with (A-B) **ER-Oct** and (C-D) ER Tracker Red (E) intensity vs. time plot demonstrating the photostability of ER-Tracker Red and **ER-Oct** obtained from the time-lapse imaging.

Subcellular fractionation of live cells for ER isolation:



Scheme S2: Schematic representation of subcellular fractionation for ER isolation from live BHK-21 cells.

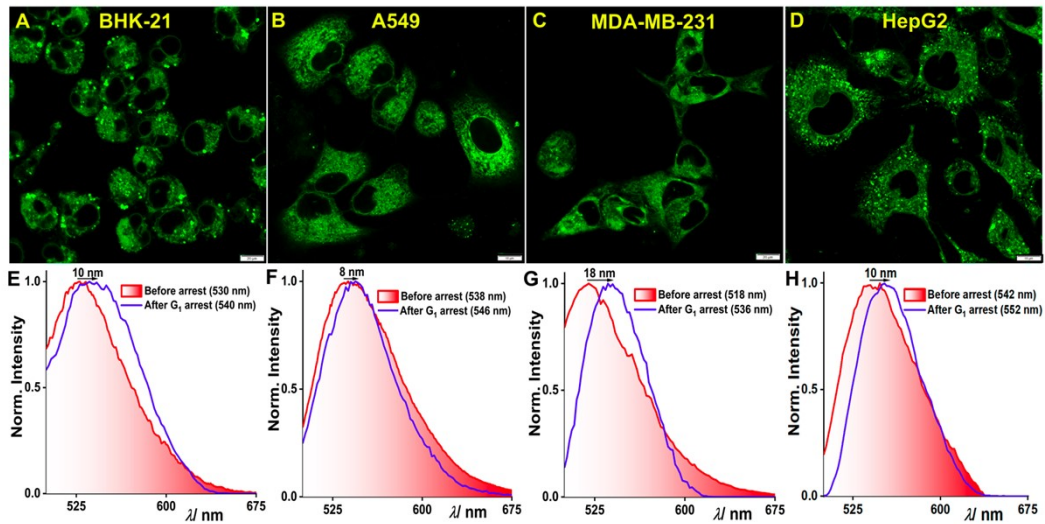


Fig. S22. ER micropolarity in G₁-phase cell cycle arrest. CLSM images of (A) BHK-21, (B) A549, (C) MDA-MB-231, and (D) HepG2 cells incubated with 2 μ M ER-Oct; (E), (F), (G), and (H) show the corresponding emission spectra recorded inside cells in lambda scanning mode (scale bar: 20 μ m). The shaded red area and blue line denote the spectra of ER-Oct inside ER before and after G₁-phase arrest [$\lambda_{ex}/\lambda_{em}$ = 488 nm/500 – 540 nm, laser power: 0.2 %, dwell time: 8 μ s/pixel, confocal aperture: 1 AU; for lambda scanning: $\lambda_{ex}/\lambda_{em}$ = 488 nm/500 – 675 nm].

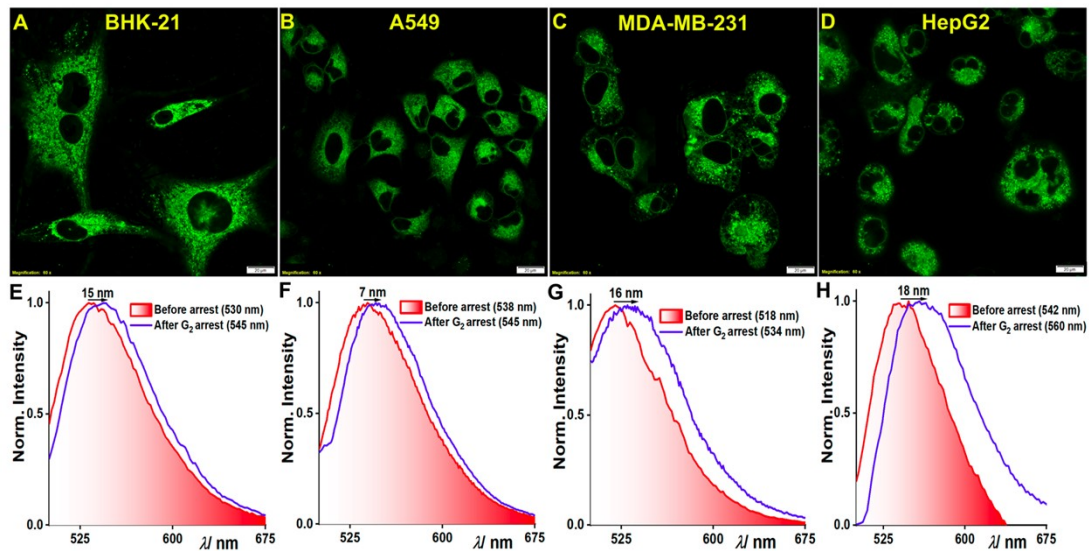


Fig. S23. ER micropolarity in G₂-phase cell cycle arrest. CLSM images of (A) BHK-21, (B) A549, (C) MDA-MB-231, and (D) HepG2 cells incubated with 2 μ M ER-Oct; (E), (F), (G), and (H) show the corresponding emission spectra recorded inside cells in lambda scanning mode (scale bar: 20 μ m). The blue line denotes the spectra of ER-Oct in water and the red line with a shaded area denotes spectra inside the ER [$\lambda_{ex}/\lambda_{em}$ = 488 nm/500 – 540 nm, laser power: 0.2 %, dwell

time: 8 μ s/pixel, confocal aperture: 1 AU; for lambda scanning: $\lambda_{ex}/\lambda_{em} = 488 \text{ nm}/500 - 675 \text{ nm}$].

Z-scanning of tumoroids and mice tissue section:

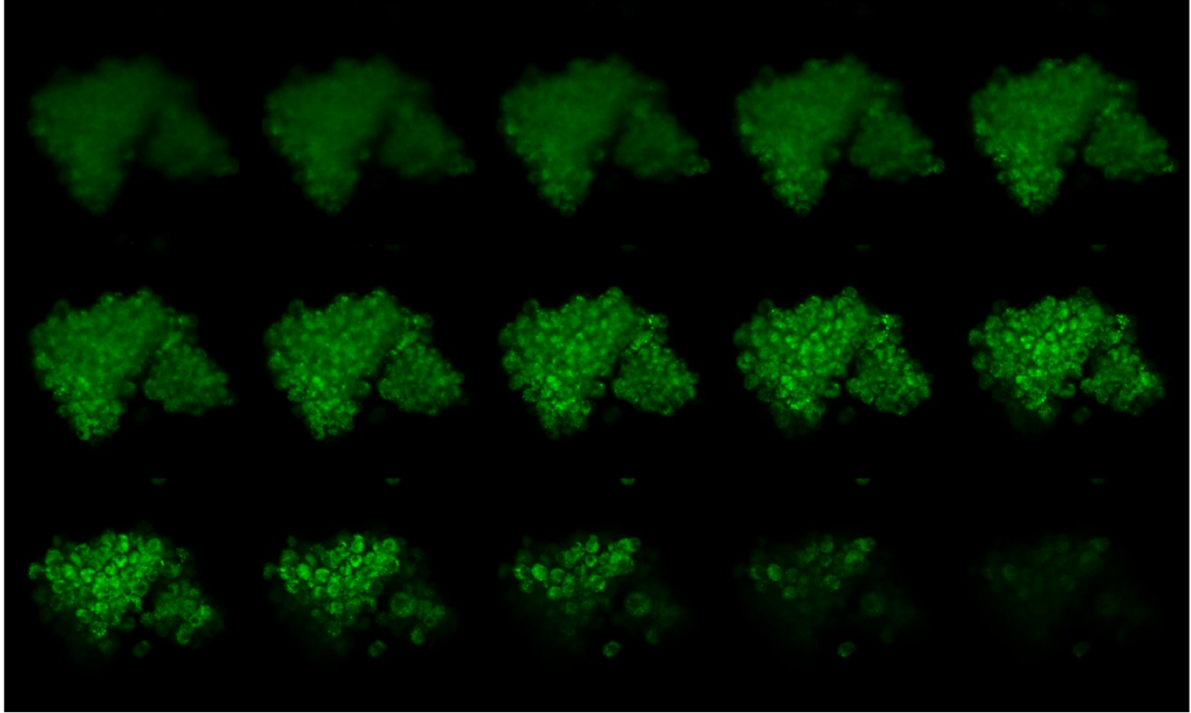


Fig. S24. CLSM Z-section images of tumoroids grown from BHK-21 cells and stained with 2 μ M ER-Oct.

ER to Golgi transport in live HeLa cells:

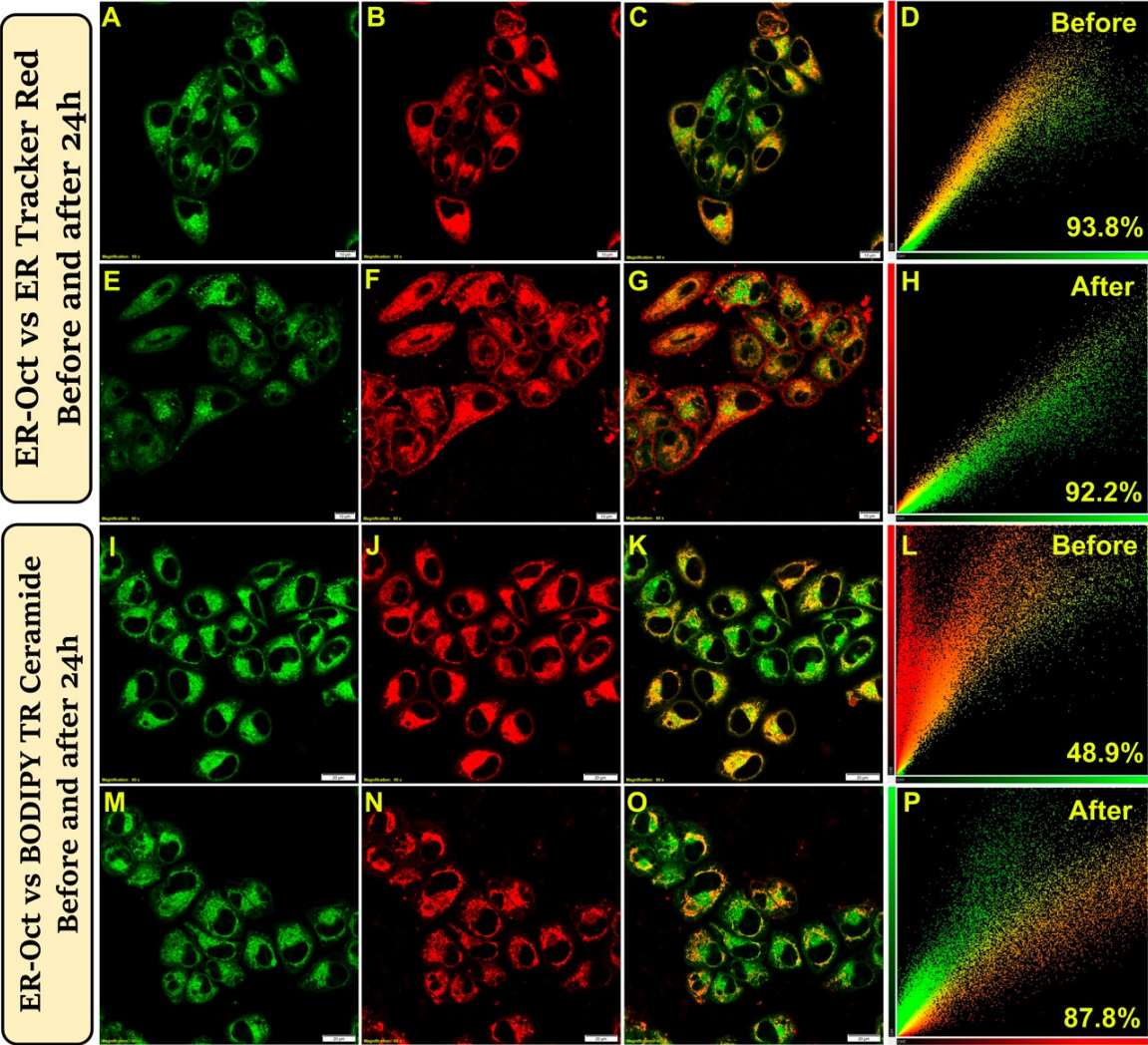


Fig. S25. CLSM images show the transport from ER to Golgi in HeLa cells. The first and third rows show images taken immediately after 10 min staining. The second and fourth rows show images taken after 24 h of 10 min staining. Images (A, E, I, M) are stained with 2 μ M ER-Oct, (B, F) are stained with 0.3 μ M ER Tracker Red, (J, N) are stained with BODIPY TR Ceramide; (C, G, K, O) are merge images, (D, H, L, P) are the corresponding scatter plots (scale bar = 20 μ m).

Micropolarity in Golgi bodies

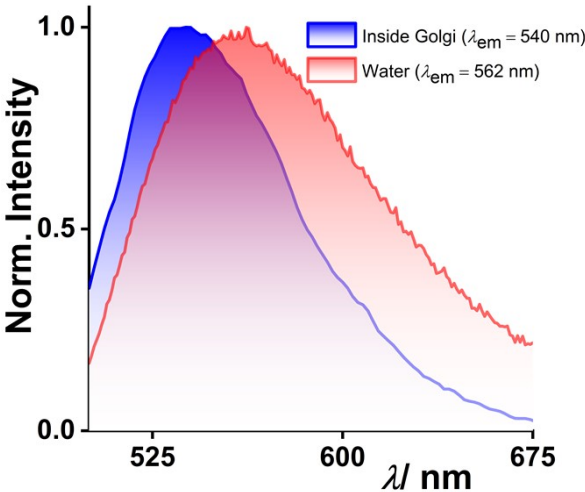


Fig. S26. Emission spectra of ER-Oct ($\lambda_{ex} = 488$ nm) inside the Golgi apparatus of BHK-21 cell line and compared with the emission spectra in water.

Inhibition of ER to Golgi transport:

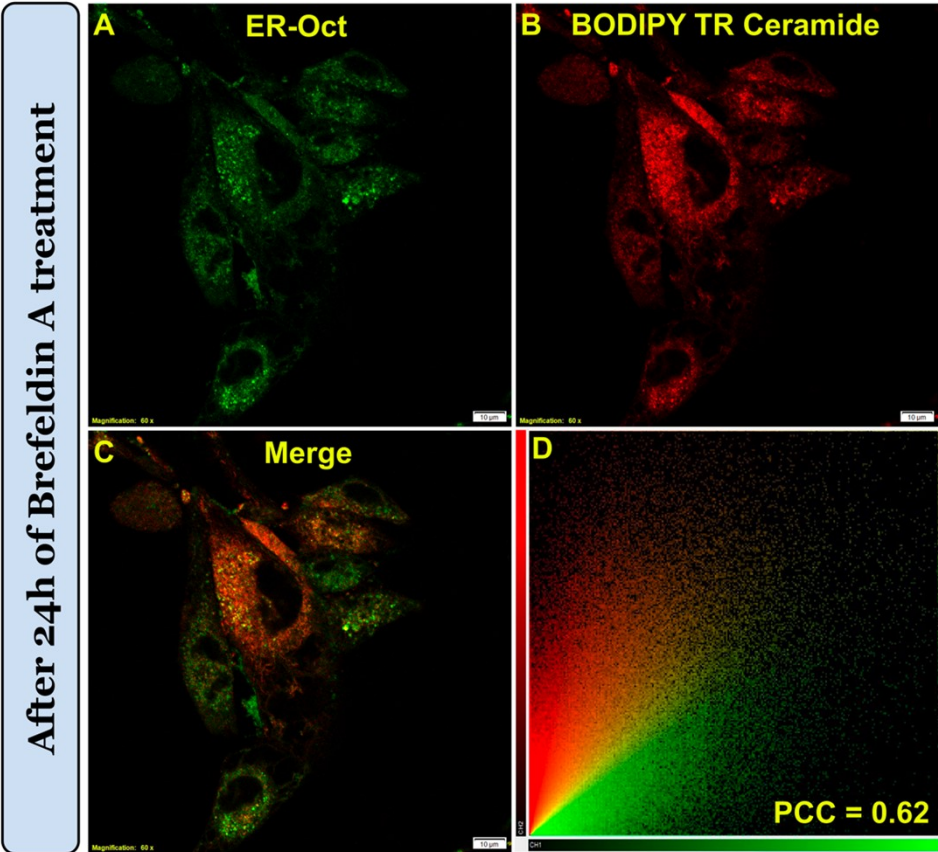



Fig. S27. CLSM images show the inhibition of the transport from ER to Golgi in live BHK-21 cells after 24 h Brefeldin A treatment. (A) 2 μ M of ER-Oct, (B) 0.3 μ M of BODIPY TR Ceramide (C) merge image of (A) and (B), (D) corresponding scatter plot with Pearson’s correlation

coefficient 0.62 ± 0.02 . The cells were treated with $5 \mu\text{M}$ Brefeldin A for 24h followed by the staining (scale bar: $10 \mu\text{m}$).

1. C. Reichardt, Solvents and Solvent Effects in Organic Chemistry, 3rd ed.,  Wiley-VCH, Weinheim, Chapter 7, pp 425-508, 2003.